Modellering, prediksjon og styring av slepte seismiske kabler

Jan Vidar Grindheim[1,2,3,*], Inge Revhaug[2], Egil Pedersen[4] og Peder Solheim[1]

Vitenskapelig bedømt (refereed) artikkel

Jan Vidar Grindheim et al.: Modeling, prediction and control of towed marine seismic streamers

KART OG PLAN, Vol. 78, pp. 231–246, POB 7030, NO-5020 Bergen, ISSN 0047-3278

A 3D numerical model for towed marine seismic streamers has been implemented. The solution is based on the FDM box method, which is a proven method for cable dynamics simulation problems, and tolerates large cable movements. The model has presently been extended to include lifting devices (control birds) for lateral and depth steering, a tailbuoy, tail stretch section as well as instruments and weights externally mounted on the streamer. The solution is validated by comparing with results from the commercial software Orcaflex, showing generally good agreement. Secondly, a simulation has been conducted investigating the maximum streamer deflection range in vertical and lateral dimensions for a range of bird wing angles, and additionally comparing these results when using bird force inputs instead of wing angles. The prime motivation is to develop a seismic streamer simulator including control birds, with low computational cost yet high accuracy, for the development of improved streamer steering algorithms.

Key words: towed marine seismic streamers, control birds, prediction, steering algorithms

Jan Vidar Grindheim, PhD student, Faculty of Science and Technology, Norwegian University of Life Sciences, P.O.B. 5003, NO-1432 Ås. E-mail: jg@geograf.no

Introduction

Improved operational efficiency has enhanced margins for marine seismic survey providers and increased seismic data acquisition affordable to oil companies. This study intends to improve prediction and control capability of towed seismic sensor cables (streamers). Improved prediction of streamer behavior is one aspect of improving the control capability.

Increasing numbers and lengths of streamers deployed, combined with 4D seismic requiring the replication of historic streamer positions, as well as non-traditional streamer deployment configurations such as slanted and fanned streamers, have increased the control precision and capability requirements significantly. The recent decline in oil prices has increased the efficiency requirements for offshore E&P even further in order to compete with shale oil E&P. The seismic survey line-change is an expensive operational maneuver moving the streamer spread 180° to the next acquisition line. This turn typically takes a few hours, accounting for a significant portion of the survey and accompanying costs, depending on the length of survey lines. Improved streamer control has the potential of decreasing this time consumption (Ersdal, 2004).

Streamer entanglement can occur both during a survey line and in turn, especially in unfavorable current conditions, and can result in damaged or destroyed streamers.

1. GEOGRAF AS, Strandgata 5, NO-4307 Sandnes, Norway.
* Corresponding author. E-mail: jg@geograf.no
2. Faculty of Science and Technology, Norwegian University of Life Sciences (NMBU), P.O.B. 5003, NO-1432 Ås, Norway.
3. Laboratório de Ondas e Correntes (LOC) at UFRJ/COPPE, Federal University of Rio de Janeiro, Rio de Janeiro 22241-160, Brazil.
4. Department of Engineering Science and Safety, UiT - The Arctic University of Norway, Hansine Hansens veg 18, NO-9037 Tromsø, Norway.

Optimal streamer steering is an important tool for avoiding streamer tangles. Given the high cost of seismic streamers and survey down-time, the relatively low cost of improvements to streamer steering algorithms are a sensible investment.

Until approximately 2000, depth control was achieved with externally mounted streamer devices where horizontal oriented wings (hydrofoils) provided the control forces (Fig. 1). By 2010, lateral steering was embraced industry wide with the development and deployment of various types of lateral steering devices. These devices, containing between two and four wings, give force in both vertical and lateral directions, and are generally referred to as "control birds" (Fig. 3).

Lateral steering enables narrow intra-streamer separations by reducing the likelihood of streamer entanglement. Less lateral streamer separation increases crossline sampling resolution. Additionally, monitoring of existing reservoirs using 4D-seismic has become increasingly important (Polydorides et al., 2008). The intention is to increase the oil reservoir recovery rates. In 4D seismic, the aim is to replicate streamer positions from historic surveys to detect changes in the reservoir caused by production. Therefore, accurate lateral control is increasingly important. Thirdly, as more complicated streamer configurations are employed, efficient real time 3D streamer control is imperative (Polydorides et al., 2008). One example of newly employed survey strategies is coil shooting, where covering of the survey area is achieved by steering the vessel in large circular paths (Buia et al., 2008). Prediction of future streamer state is one important aspect of improved streamer steering algorithms (Solheim, 2013).

As prescribed by International seagoing laws, the tail end of each streamer is identified to non-survey vessel traffic by a tailbuoy towed from each streamer. This tailbuoy ensures tail-end tension and provides a platform for navigation instruments such as acoustic pingers, compasses and satellite navigation systems. A stretch section is installed between the last streamer section and the tailbuoy, to dampen tugging noise on the streamer. Streamer positions are determined with the use of streamer mounted instruments that determine distances (acoustically), magnetic directions (compasses) and Global Navigation Satellite Systems (GNSS) navigation control points installed at the tailbuoys, streamer front buoys and at the vessel.

Ballasting to bring the streamer to the desired depth is achieved by attaching weights along the streamer. Lead weights are installed to balance the streamer sections as salinity may vary at the survey prospect. Hence, ballasting reduces the workload on depth keeping birds and gives consistent cable depth between depth control bird locations. All streamer add-ons, whether instruments inserted between streamer sections or

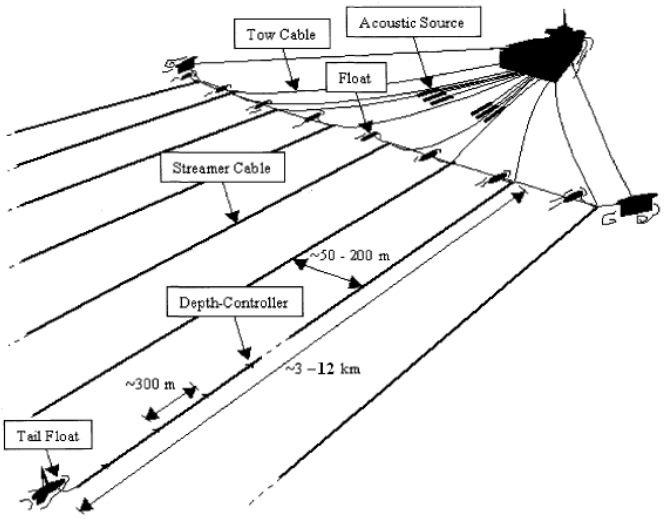

Fig. 1: Illustration of seismic spread with installed devices from Pedersen (2001).

attached to streamer coils, or weights clamped onto the streamer body, typically have densities much larger than the streamer, thus affecting the vertical shape of the streamer significantly (Grant, 2015). Their drag properties also differ from the streamer, affecting the lateral streamer shape.

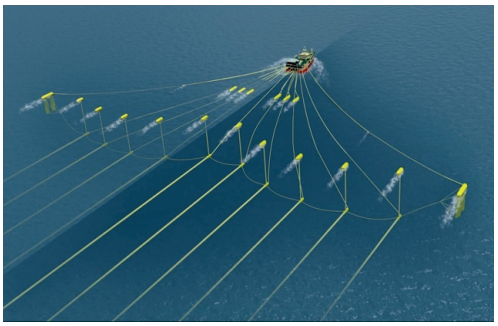

Fig. 2: Example of seismic streamer towing configuration (courtesy of Petroleum GeoServices).

Within the seismic industry, various streamer control devices have been developed. Kongsberg Seatex has developed the eBird® streamer steering device for combined roll, depth and lateral control, which is an in-line control unit with 3 wings (Seatex, 2013a) (Fig. 3).

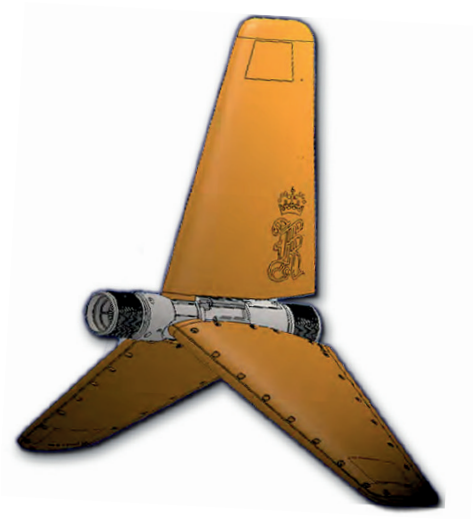

Fig. 3: Kongsberg Seatex eBird® for lateral steering and depth control of seismic streamers (Seatex, 2013b).

In the present article, a novel seismic simulator is described. The model is in three dimensions and includes cable stretch and tension. It is solved using a Finite Difference Method (FDM). Control birds are included in the simulator, as well as a tailbuoy which is constrained to the surface using a PID controller. It is custom-tailored to simulate seismic streamers, hence implementation of a specific seismic design is straight-forward for the user. As the code is implemented in Matlab® (Matlab), it can easily be combined with other codes or technologies, for instance the Ensemble Kalman Filter (Grindheim et al., 2017). It can also be customized further according to user specifications.

Towed underwater 3D cable model

For studying the behavior of a buoyant streamer, a three-dimensional cable dynamics model is required (Grant, 2015). Ersdal (2004) concluded that for simulation of "maneuvering and special operation" of the complete seismic spread, "an effective three dimensional model of a cable that allows high deformation" would be necessary. Such a model has been implemented.

The streamer's dynamics can be adequately described by six coupled nonlinear partial differential equations (Burgess, 1991, Grindheim et al., 2017):

$$\mathbf{M}\frac{\partial \mathbf{y}}{\partial s} = \mathbf{N}\frac{\partial \mathbf{y}}{\partial t} + \mathbf{q} \tag{1}$$

where

$$\mathbf{y} = \begin{bmatrix} T & v_t & v_n & v_b & \theta & \varphi \end{bmatrix}^{\mathrm{T}} \tag{2}$$

and

$$\mathbf{M} = \begin{bmatrix} 1 & 0 & 0 & 0 & 0 & 0 \\ 0 & 1 & 0 & 0 & v_b\cos\varphi & -v_n \\ 0 & 0 & 1 & 0 & -v_b\sin\varphi & v_t \\ 0 & 0 & 0 & 1 & v_n\sin\varphi - v_t\cos\varphi & 0 \\ 0 & 0 & 0 & 0 & -T\cos\varphi & 0 \\ 0 & 0 & 0 & 0 & 0 & T \end{bmatrix} \tag{3}$$

$$\mathbf{N} = \begin{bmatrix} \frac{-mv_t}{E_A+T} & m & 0 & 0 & m_1 v_b \cos\varphi & -m_1 v_n \\ \frac{1}{E_A} & 0 & 0 & 0 & 0 & 0 \\ 0 & 0 & 0 & 0 & 0 & 1+\frac{T}{E_A} \\ 0 & 0 & 0 & 0 & -\left(1+\frac{T}{E_A}\right)\cos\varphi & 0 \\ \frac{-m_1 v_b}{E_A+T} & 0 & 0 & m_1 & m_1 v_n \sin\varphi - mv_t \cos\varphi & 0 \\ \frac{-m_1 v_n}{E_A+T} & 0 & m_1 & 0 & -m_1 v_b \sin\varphi & mv_t \end{bmatrix} \tag{4}$$

and **q** is a 6x1 vector accounting for hydrodynamic and buoyancy forces:

$$\mathbf{q} = \begin{pmatrix} \frac{1}{2}\rho d\pi C_t \left(1+\frac{T}{E_A}\right)^{\frac{1}{2}} |V_t| V_t + (m-\rho A) g \sin\varphi \\ 0 \\ 0 \\ 0 \\ \frac{1}{2}\rho d C_n \left(1+\frac{T}{E_A}\right)^{\frac{1}{2}} V_b \left(V_n^2 + V_b^2\right)^{\frac{1}{2}} \\ \frac{1}{2}\rho d C_n \left(1+\frac{T}{E_A}\right)^{\frac{1}{2}} V_n \left(V_n^2 + V_b^2\right)^{\frac{1}{2}} + (m-\rho A) g \cos\varphi \end{pmatrix} \tag{5}$$

T is tension, v is velocity, and t, n and b are tangential, normal (nadir) and bi-normal vectors, respectively (Fig. 4). θ and φ are horizontal and vertical angles, respectively, between tangent t and the x-vector (Fig. 4). E is cable elasticity, A is cable cross-sectional area, $E_A = EA$, V is velocity relative to surrounding fluid, i.e. $V_t = v_t - U_t$, $V_n = v_n - U_n$ and $V_b = v_b - U_b$. m is cable mass per unit length, m_1 is cable mass including added mass, per unit length, ρ is fluid density, g is gravity constant, C_t is tangential drag coefficient, C_n is drag coefficient for both n- and b-directions, and d is cable diameter.

The model uses a local coordinate system following the cable tangent t (Fig. 4), as this simplifies the equations. v (ms^{-1}) is velocity, T is cable tension (N), and θ and φ are angles as given in Fig. 4.

There are three equations resulting from the cable kinematics, essentially starting from the equation for cable strain (Eqn. (6)) and the rotation matrix from absolute to local (t,n,b) coordinate system.

$$\frac{\partial p}{\partial s} = 1 + \frac{T}{E_A} \tag{6}$$

where p and s are stretched and unstretched cable lengths, respectively. (T / E_A) equals cable strain, with $E_A = E \cdot A$, where E is elasticity, and A is the cross sectional cable area (m^2): $A = \pi(d/2)^2$. d is cable diameter (m).

Secondly, there are three equations resulting from the equilibrium of forces, where cable tension distance derivative $\left(\partial\vec{T} / \partial s\right)$ equals the sum of inertial ($\vec{F}_i$), hydrodynamic ($\vec{F}_h$) and buoyancy ($\vec{F}_w$) forces:

$$\frac{\partial \vec{T}}{\partial s} = \vec{F}_i + \vec{F}_h + \vec{F}_w \tag{7}$$

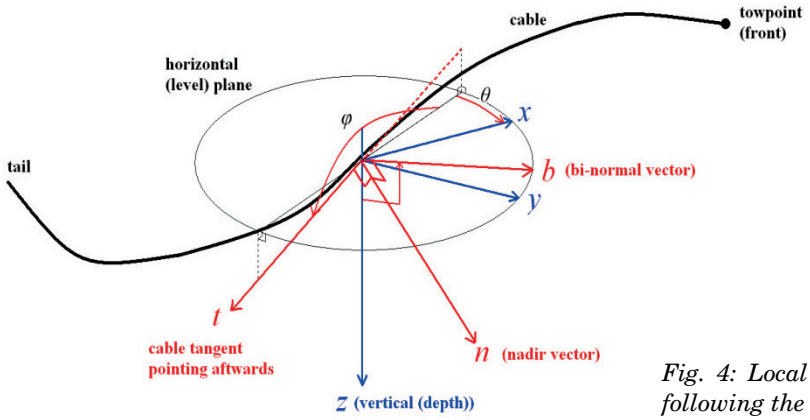

Fig. 4: Local coordinate system following the cable tangent t.

Variations of the model have been utilized by numerous authors (Gobat and Grosenbaugh, 2006). The model includes cable tension, cable stretch and ocean current which can vary along the cable, and it tolerates large cable deflections.

The boundary conditions are:

- Known velocity at front
- Known tension at tail and assuming straight cable at tail point.

Solving the equations

The equations (1) are solved using the box method, which is a Finite Difference Method (FDM). The solution was introduced by Ablow and Schechter (1983) and improved by Milinazzo et al. (1987) and Burgess (1991). Newton-Raphson iteration is used for solving the next timestep. The box method gives second order accuracy and allows for arbitrary, i.e. non-uniform, spacing in time and space, and allows for rapid variations in time step size (Cebeci et al., 2005). The discretization is centered in time and space. The method has proven close match with full-scale data and low computational cost (Burgess, 1991). Further details of the method are presented in Grindheim et al. (2017).

The solution is stable for long time steps, typically in the order of 20 seconds, resulting in fast integration time. For seismic surveys, typically update timesteps is in the order of 10 seconds, which is well within the stability timestep size. Nodes or control birds could be placed at any point along the cable. Implementation has been performed in Matlab® (Matlab).

For realistic simulations of seismic streamers, several additional features have been added to the model:

- Control birds have been added. The hydrodynamic bird forces are added as an extra current vector $[U_{t\_bird}\ U_{n\_bird}\ U_{b\_bird}]$ at the two cable elements adjacent to each bird. This extra current is calculated to give the force corresponding to the bird force given the state, including velocity and current vectors, at present time. The reason for this choice and the details of the procedure will be explained.
- A tailbuoy has been added. Using boundary condition at tail $v_z = 0$ was attempted, but instability issues occurred. Instead, a tailbuoy vertical buoyancy force is added at the tail, with a PID-controller controlling this vertical force for keeping *depth* = 0. In addition, a short cable section of large diameter following the tail is added to account for the tailbuoy drag.
- Components with specified weight in water and diameter can be installed at user defined locations. Nominal component length is 1 meter.
- A stretch section of user defined length is installed prior to the tailbuoy, connecting the tailbuoy and streamer.

Example of a simulation plot is presented in Figs. 5–6. Control birds are marked with green dots, and the red dot is the tailbuoy.

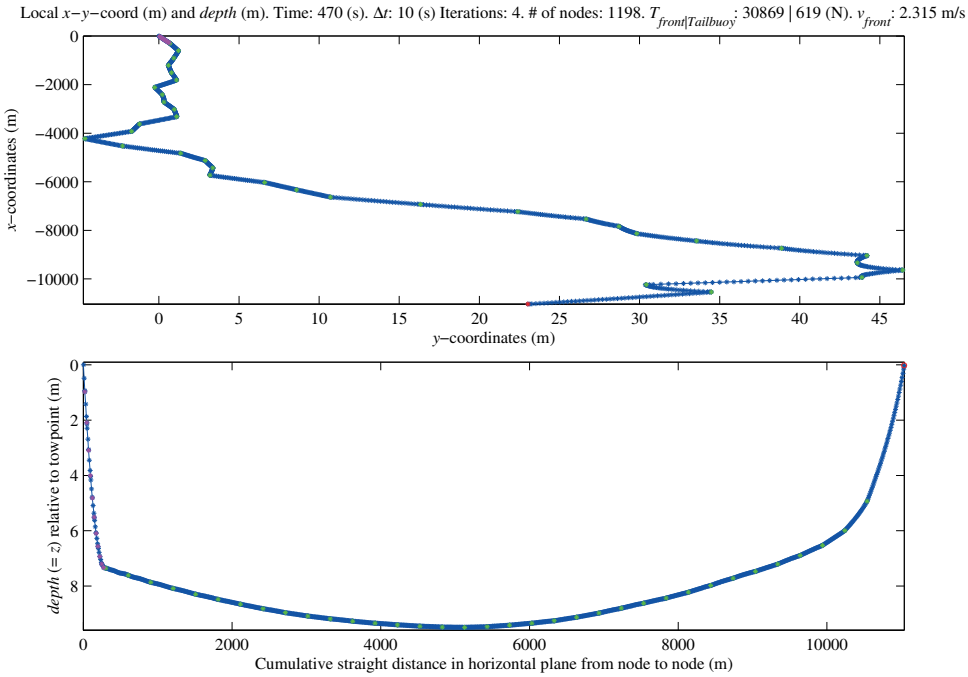

Fig. 5: Example of simulation plot. The red dot is the tailbuoy, the green dots are control birds and components are marked with magenta dots. Note the large variations in axis scales.

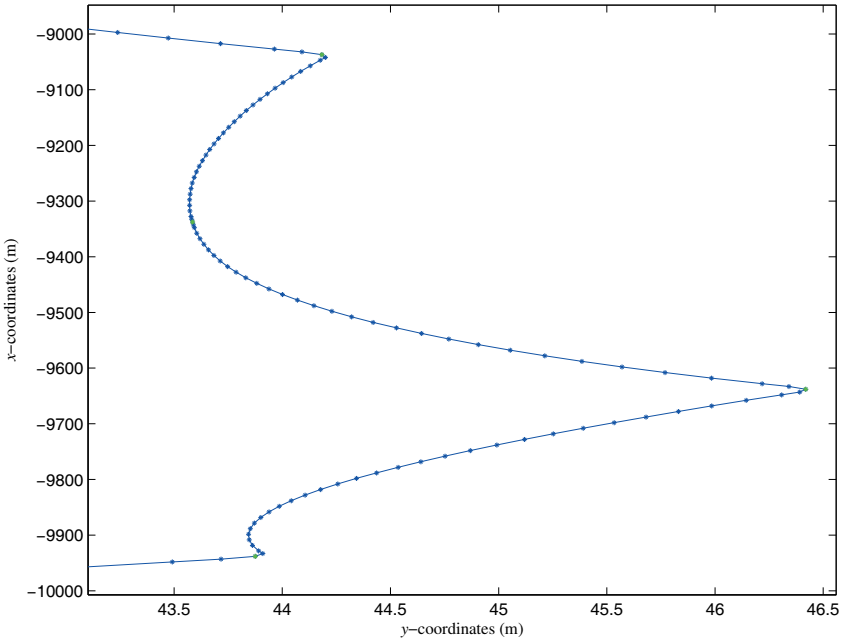

Fig. 6: Close-up of the x-y coordinate plot in Fig. 5, showing three steering birds. Note the large difference in scale between x- and y-axis.

Implementing control birds

The control birds have been added to the original model (Eqn. (1)). For each bird, two cable segments, each of equal unstretched length (default value 5 m), are included adjacent to the bird. The bird inputs could be given as wing deflections (degrees) and wing orientation (degrees), or directly as force (N) in n- and b-direction. For the bird wing deflection option, the force calculation procedure is given in the following.

Hydrofoil force calculation

Hydrofoil forces are calculated based on the actual wing angle of attack with respect to wing deflection, local bird velocity and sea current.

Lift- and drag curves are implemented for a basic symmetric wing profile. It is assumed a maximum lift coefficient $\partial CL(\alpha)/\partial\alpha\,|_{\alpha=15^\circ} = 0.7$, where α is the angle between incoming fluid stream and hydrofoil chord line. The coefficient is linear with angle of attack until close to stall angle, where the lift decreases (Fig. 7). For simplicity, a rate of decrease in C_L is assumed after stall that is equal to the rate of C_L increase before stall (Fig. 7). The hydrofoil is symmetric, giving equal lift- and drag coefficients for both positive and negative angles of attack.

The drag coefficient C_D is the sum of the friction coefficient and the pressure drag coefficient, where the friction coefficient is constant, and the pressure drag coefficient is assumed to depend on α only (Newman, 1977, p. 23). At $\alpha = 0°$, C_D approximately equals the friction coefficient, whereas the assumption is that the remaining drag, i.e. the pressure drag, depends only on angle of attack (Newman, 1977, p. 23). Friction drag could be approximated by friction drag C_F of a flat plate at zero angle of attack (Newman, 1977, p. 23). Assuming wing chord length of 0.3 m and towing speed 2.4 ms^{-1}, typical for seismic operations, this gives friction coefficient $C_F = 0.0055$ (Newman, 1977, p. 17).

Based on these notions, idealized Fourier series curves have been developed for both C_L and C_D as functions of angle of attack α (James et al., 2011, pp. 571-575). The curves with their derivatives are shown in Fig. 7. For calculating C_L, $\mathrm{N}_{\mathrm{Fourier}}$ (Fourier series length) has been set to 20, while for C_D, $\mathrm{N}_{\mathrm{Fourier}} = 6$ has been utilized. One advantage of using Fourier series is that its derivative is continuous, which would not be the case if a piecewise function was utilized. The described Fourier series lift- and drag coefficient calculation routines are utilized in the function calculating hydrodynamic force for bird wings.

The code calculates hydrodynamic forces for each hydrofoil based on relative fluid velocity, deflection and orientation of wing, wing area, fluid density and stall angle (Newman, 1977). The results are L (lift) and D (drag).

Subsequently, the force vector is rotated by angle $(\beta–\alpha)$ to generate F_t (force in cable tangent direction) and F_{bn} (force in b–n-plane, i.e. 90° to cable tangent) (Fig. 8). This is because by definition, the drag component is in the direction of the fluid velocity, and the lift is perpendicular to the drag (Newman, 1977, p. 21).

From F_{bn}, the F_b and F_n components are calculated based on orientation angle of the bird. The calculated forces are then implemented as additional forces in the **q**-vector, Eqn. (5), at the two cable elements adjacent to the birds.

The bird forces are represented by additional currents added only at the two cable elements adjacent to the bird. The additional currents are calculated to give the correct resultant **q**-vector force at the bird elements, i.e. the resultant force of hydrodynamic, gravitational and buoyancy, and bird force. The reason for this choice is issues with stability and convergence experienced when attempting to implement the bird forces explicitly in the **q**-vector, Eqn. (5). One reason for stability issues may be the high sensitivity of the bird force with respect to wing angle of attack.

The bird force currents are updated each shotpoint given the present state. The bird force calculations are decoupled from the Newton iteration, leading to a time lag. However, the time lag should be reasonable small as the forces are updated each shotpoint. If higher accuracy is desired, the timestep size could be reduced by user. The non-linear interaction between the cable velocity, sea current and control forces will still be accounted for, but with a time lag and approximation.

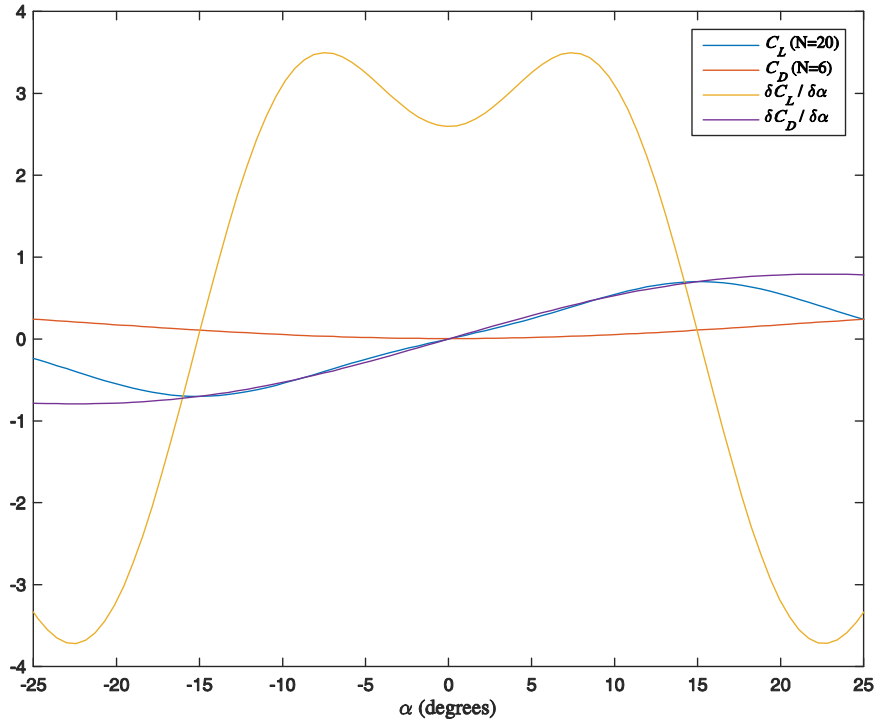

Fig. 7: Idealized Fourier series curves for both C_L and C_D (as functions of angle of attack α), as well as their derivatives.

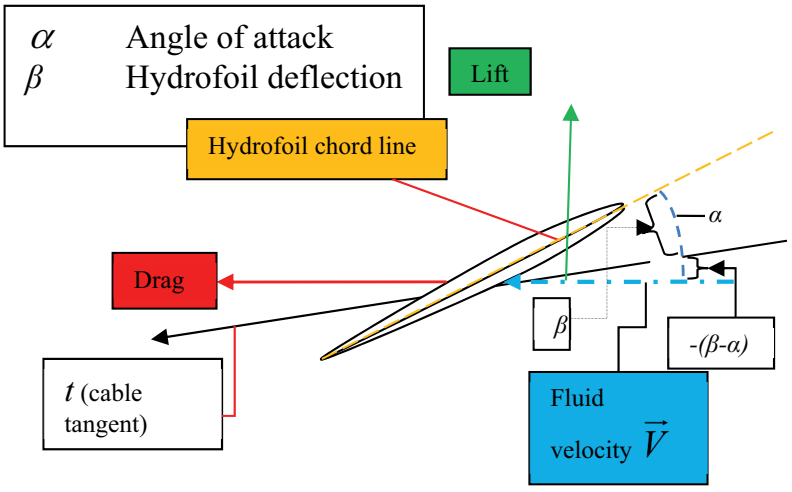

Fig. 8: Hydrofoil with angles, vectors and explanations.

The added bird force currents are calculated based on the hydrodynamic force equations given in the **q**-vector (Eqn. (5), elements 1, 6 and 5, respectively).

For calculating the bird force currents, tangential force current U_{t_bird} is calculated based on:

$$F_t = \frac{1}{2}\rho d\pi C_t\left(1+\frac{T}{E_A}\right)^{\frac{1}{2}}\left|v_t - U_{t\_bird}\right|\left(v_t - U_{t\_bird}\right) \quad (8)$$

Bi-normal and normal force currents U_{b_bird} and U_{n_bird} are calculated from Eqn. (9) and Eqn. (10), respectively, using least squares method.

$$F_b = \frac{1}{2}\rho dC_b\left(1+\frac{T}{E_A}\right)^{\frac{1}{2}}\left(v_b - U_{b\_bird}\right)\left(\left(v_n - U_{n\_bird}\right)^2 + \left(v_b - U_{b\_bird}\right)^2\right)^{\frac{1}{2}} \quad (9)$$

$$F_n = \frac{1}{2}\rho dC_n\left(1+\frac{T}{E_A}\right)^{\frac{1}{2}}\left(v_n - U_{n\_bird}\right)\left(\left(v_n - U_{n\_bird}\right)^2 + \left(v_b - U_{b\_bird}\right)^2\right)^{\frac{1}{2}} \quad (10)$$

The extra current [U_{t_bird} U_{n_bird} U_{b_bird}] representing the bird force is added to the sea current at the two short cable elements adjacent to the bird.

Validation of implementation

The streamer simulation implementation has been verified against a simulation performed with Orcaflex®, a commercial software for hydrodynamic simulations (Orcina, 2016).

The development of the present simulator was justified by the following requirements that are not met by Orcaflex:

1. Generic initialization customized for seismic streamer simulation.
2. Optimized cycle time for seismic streamer problem.
3. In-house control of all aspects of the simulator and underlying model, and further development of any desired extensions, modifications or improvements.

In the Orcaflex verification run, the simulated cable is a seismic streamer of unstretched length 7800 m, diameter d = 6 cm and neutral weight in water, resulting in constant depth of the cable. The complete cable has uniform cable properties. Towpoint tension (total drag including cable, wings and tailbuoy) is 20.9 kN at 4.5 knots (2.315 m/s) with wings not activated. The cable has 25 birds with 300 m spacing between each. 25 simulations are run, where for each simulation, only one of the birds are activated, giving constant lateral force of 270 N. Timestep size is 10 seconds. The resulting cable shape from one of the simulations (activating bird number 5) is given in Fig. 9.

The accuracy of the FDM method is dependent on number of cable nodes; hence there is a tradeoff between accuracy and computational cost. Computational cost of the algorithm increases in a linear fashion with number of nodes. With distance between cable nodes at 10 meters, each 200 second simulation takes ca. 1.3 seconds on a standard laptop, decreasing to ca. 0.5 seconds for 50 meters between the cable nodes. The simulation results for distance between nodes at 10, 25, 50 and 100 meters, as well as the Orcaflex simulation results, are presented in Fig. 10. Generally, good agreement with the Orcaflex result is achieved, but towards the end of the cable, the agreement decreases for the larger distance between cable nodes (Fig. 10). The deflection trend shows that the closer to the towpoint, the less the deflection will be (Fig. 10). Close to the tailbuoy, the tailbuoy drag will constrain the cable.

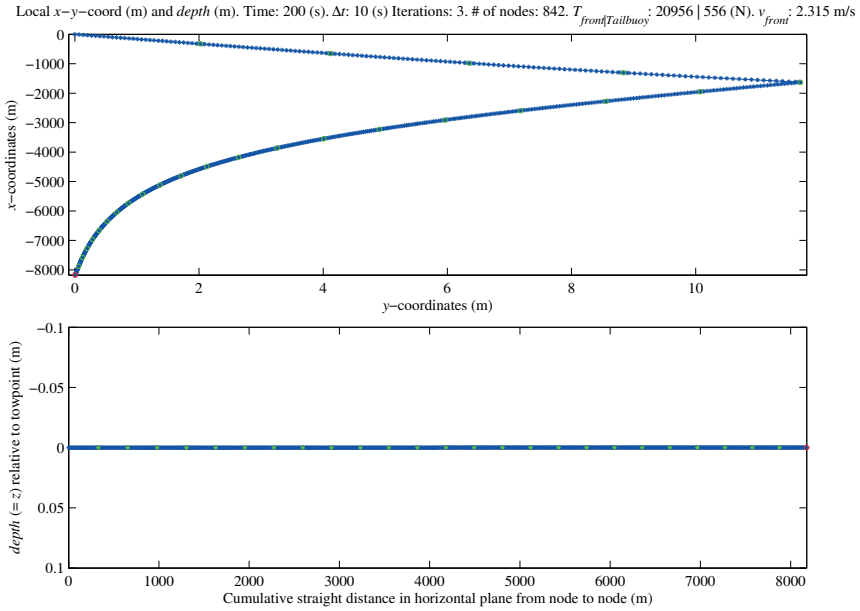

Fig. 9: Sample plot – bird number 5 is activated; cable deflection after 200 seconds is shown. Distance between nodes is 10 m. Note the difference in scale between x- and y-axis for the lateral (upper) plot. Note the differences in axis scales.

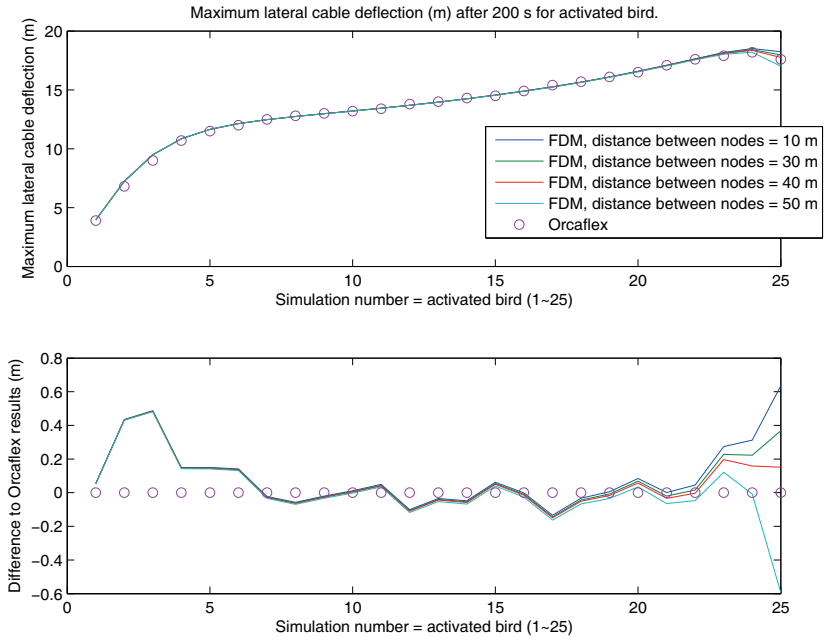

Fig. 10: Results of the 25 simulations, comparing FDM code results for different number of cable nodes, with the Orcaflex result. For each simulation only one of the control birds is activated, and the cable deflection at the bird after 200 s is given in the figure. Bird number 1 is closest to the front, and bird number 25 is closest to the tail. Upper plot shows absolute results, lower plot shows relative results in relation to the Orcaflex results.

Exploring control ranges and correlation between lateral and vertical steering

A simulation study has been developed to determine the possible ranges of lateral and depth control, as well as their correlations, when controlling both simultaneously. Estimating this is not straight-forward, as many factors contribute to the results. For instance, as the cable is moved out in the lateral, the wing angles of attack will change, and as the wings' angle of attack approaches the stall angle, the stall effects will influence the results. Secondly, steering in the vertical could influence the steering in the horizontal, and vice versa.

The streamer has length 7800 m, diameter 6 cm, weight in water of 0 N/m, and each bird has a weight in water of 2.5 N. 24 birds are installed with spacing 300 m. Each bird has two wings of surface 0.208 m^2, one oriented horizontally (giving force in the vertical when activated) and one oriented vertically (giving horizontal force when activated). Wing area is set to give a lift force at stall angle of 400 N at nominal speed 2.315 ms^{-1}. A stretch section with length 100 m is installed 500 m after the last bird. The stretch section connects the streamer to the tailbuoy.

Prior to the front bird, 11 weights of 100 N each are installed with equal spacing. This is a standard operational practice to make the front section of the streamer stay closer to the target depth. Nominal towpoint tension with birds not activated is 21.47 kN. Streamer shape at simulation time zero is a steady state solution with zero bird forces, as presented in Fig. 11.

A number of 20 minute simulations have been run. The towpoint is running straight ahead at 2.315 m/s. For each simulation run, wing deflections are constant for all 24 birds. The extreme cable deflection (i.e. the largest deflection, positive or negative, at any node) after 20 minutes is recorded for both vertical and lateral dimensions.

One simulation example is given in Fig. 12, where vertical force wing has deflection 4 degrees, and horizontal force wing has deflection –12 degrees.

All simulation results are presented in Figs. 13–14. Lateral force wing deflection is varied between –20 and 20 degrees, and vertical force wing between 0 and 20 degrees,

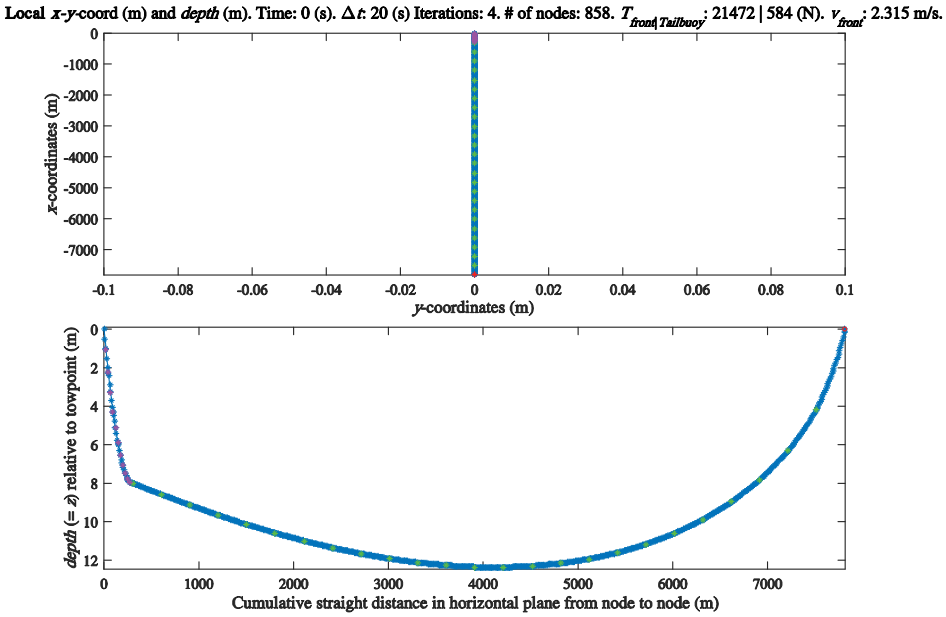

Fig. 11: Simulation streamer shape at simulation time = 0. This is the steady-state solution with no bird forces. Green dots are birds and magenta dots the installed weights. The red dot is the tailbuoy.

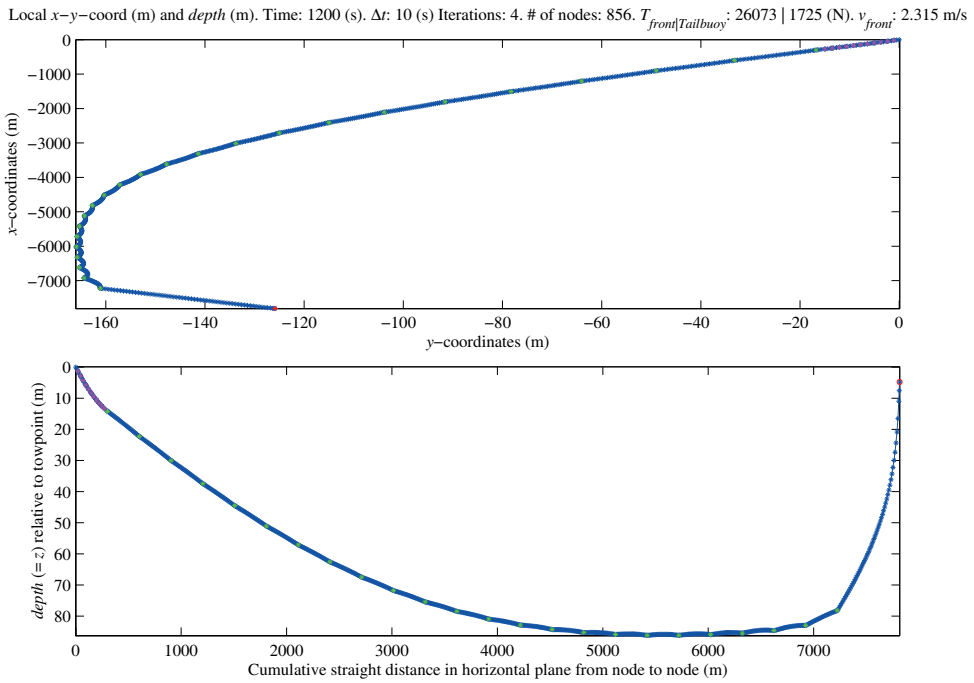

Fig. 12: Result plot for one of the 20 minute simulations. The green dots are the control birds. Magenta dots are installed weights. Note the differences in scale between x- and y-axis for both of the two plots. In this simulation, vertical force wing has deflection 4 degrees, and horizontal force wing has deflection –12 degrees.

with 1 degree resolution. Fig. 13 gives the resulting maximum vertical cable deflection, and Fig. 14 the resulting maximum lateral cable deflection, for all simulations run within the wing angles span.

Secondly, the results indicate that lateral and vertical steering are only slightly dependent on each other (Figs. 13–14). This may indicate that vertical and lateral control could be considered separately for simplicity.

Independent of the correlation between vertical and horizontal steering, since the same birds are typically utilized for both depth and lateral steering, it could be beneficial to develop a single control algorithm considering both the vertical and the lateral dimensions at the same time. 3D simulations will certainly be beneficial in the control algorithm development for buoyant streamers (Ersdal, 2004). There is a limited amount of total control force available, and the algorithm needs to determine optimal distribution of force in vertical and lateral dimensions. Further, in the field the streamers have varying buoyancy, thus requiring 3D simulations for accurate modeling (Grant, 2015).

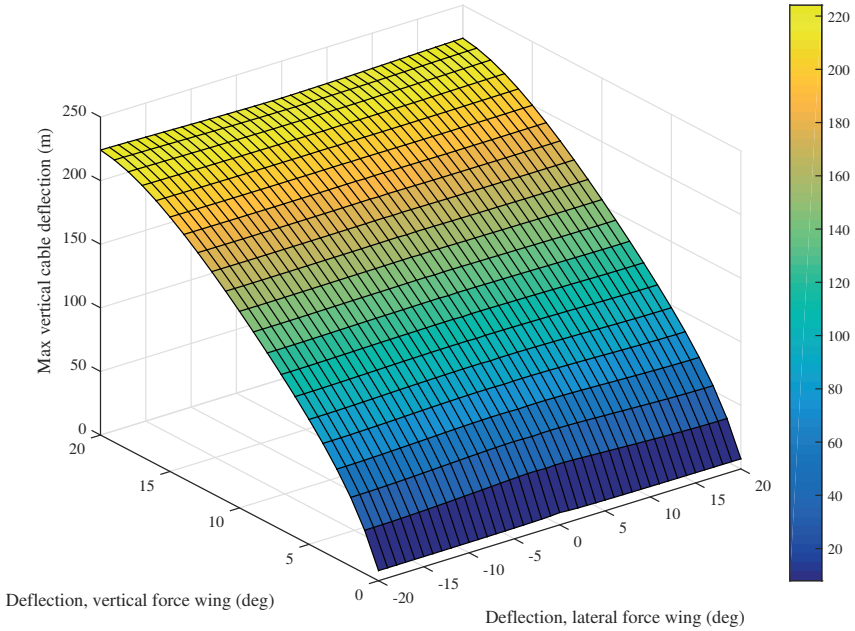

Fig. 13: Extreme vertical cable deflection after 20 minutes. For each simulation, all 25 birds are given the same wing deflections for the lateral and the vertical force wing, respectively, and the extreme (i.e the largest, positive or negative) lateral cable deflection after 20 minutes is recorded.

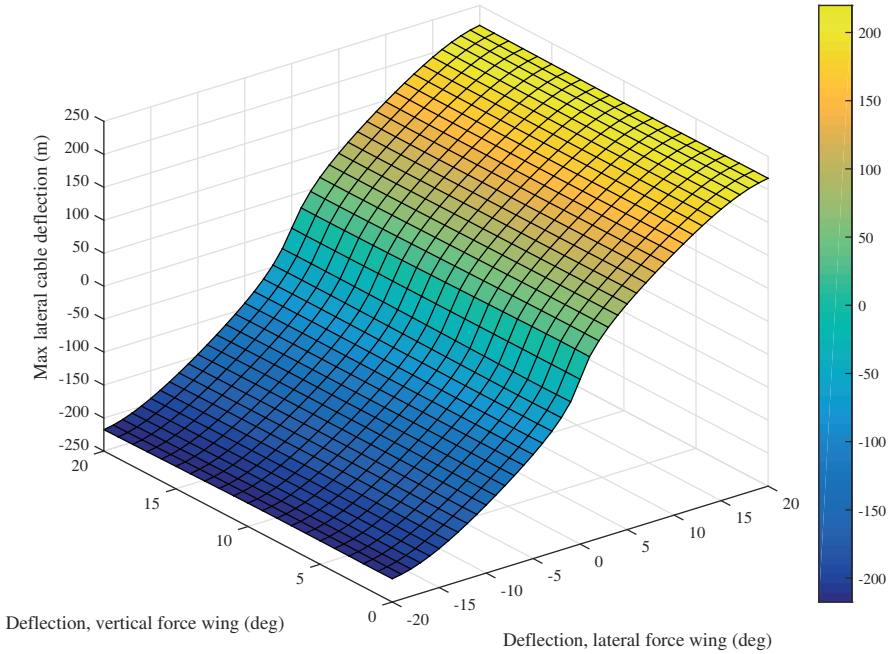

Fig. 14: Extreme lateral cable deflection after 20 minutes. For each simulation, all 25 birds are given the same wing deflections for the lateral and the vertical force wing, respectively, and the extreme (i.e the largest, positive or negative) lateral cable deflection after 20 minutes is recorded.

The same simulation has been run using known bird force input instead of control angles. In this case, maximum control force is calculated by assuming maximum available force at V_t = 2.315 ms^{-1} (4.5 knots) is equal to 400 N, which is equal to nominal force for the control wings at stall angle at nominal speed (15 deg). This gives maximum force (100 %):

$$Maxforce = \frac{400}{2.315^2} V_t^2 \qquad (11)$$

where V_t is tangential bird velocity relative to fluid. Note that this is a simplification as force is also dependent on V_n and V_b, and since maximum force in one direction is dependent on the force in the other as there is a total maximum force available for the bird. Secondly, increased streamer deflections will affect the wing angles, thus affecting available steering force. The results for the set bird force input are presented in Fig. 15–16. The results show close similarity to the results when using wing angles (Figs. 13–14), thus giving credit to the bird wing angle implementation.

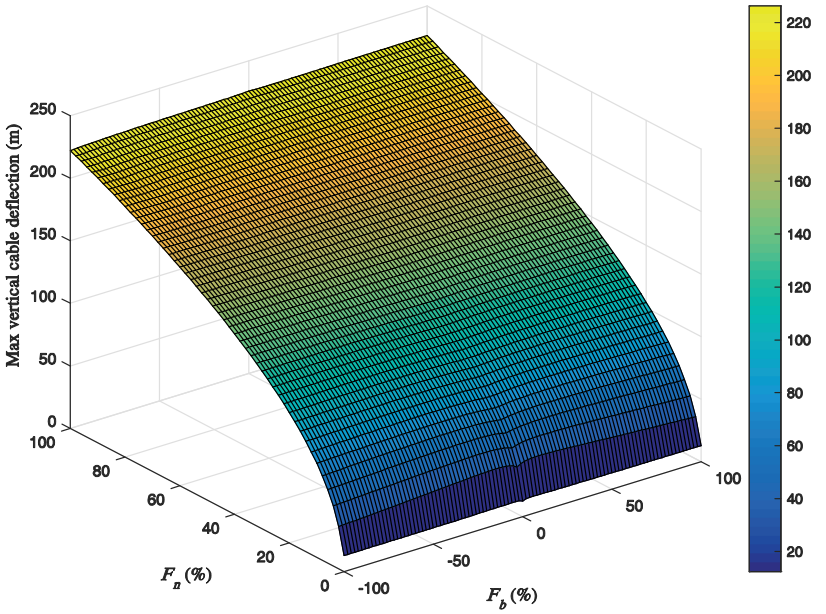

Fig. 15: Same simulation as in Fig. 13, but using known bird force input instead of wing angles. Extreme vertical cable deflection after 20 minutes. For each simulation, all 25 birds are given the same force in F_b and F_n, respectively, and extreme cable deflection after 20 minutes is recorded. (F_b is in the horizontal plane perpendicular to the cable tangent, while F_n is nadir vector perpendicular to cable tangent (Fig. 4)).

Conclusion

Present motivations for modeling and prediction of seismic streamers are related to the problem of improved streamer steering.

A 3D Partial Differential Equations (PDE) cable model for simulating towed underwater cable dynamics has been extended to include typical seismic streamer devices such as control birds, tailbuoy, tail stretch section, and weights and instruments externally mounted on the streamer. The implementations are presented. The equations are solved using the box method, a Finite Difference Method (FDM). Validation shows good

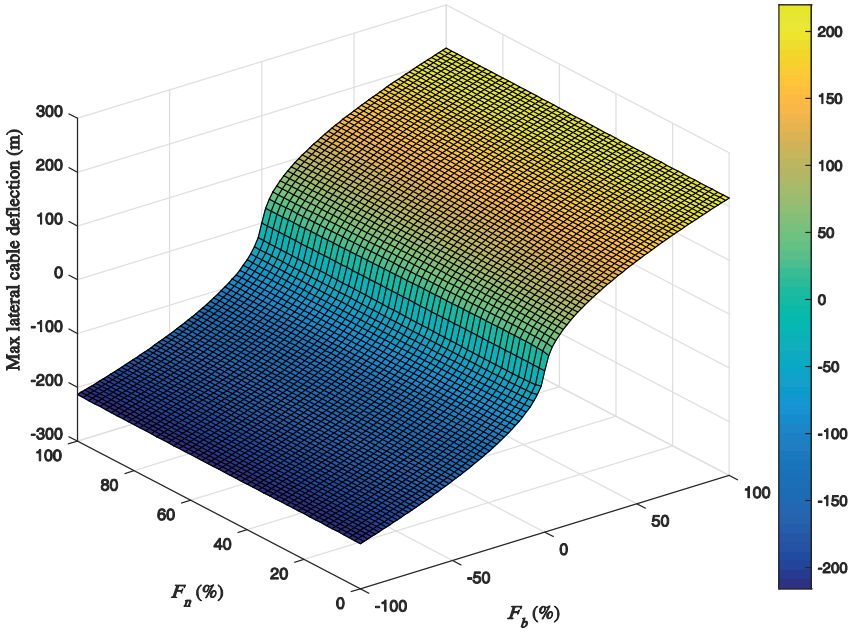

Fig. 16: Same simulation as in Fig. 14, but using known bird force input instead of wing angles. Extreme lateral cable deflection after 20 minutes. For each simulation, all 25 birds are given the same force in F_b and F_n, respectively, and the extreme (i.e the largest, positive or negative) lateral cable deflection after 20 minutes is recorded.

correspondence with simulation results from the commercial software Orcaflex. The implementation has low computational cost.

Secondly, the possible amounts of lateral and vertical steering for both a range of bird wing angles and a range of bird forces, as well as their correlations, have been explored through simulations. The results for wing angle variations generally compare well to the result for known bird force, giving a validation of the wing angle force implementation. The simulations indicate that lateral and vertical steering are only slightly affected by each other. However, typically the same birds are utilized for both depth and lateral control, and the total control force available is limited. Thus a single control algorithm considering both lateral and vertical dimensions simultaneously may be necessary for determining optimal force distribution. Utilizing 3D simulations in the development should be beneficial, especially when considering streamers that are not completely neutrally buoyant, as is normally the case.

Recommendations for further work

A simulation study comparing the control efficiency of a 2-wing and a 3-wing bird design could be of interest for the seismic industry, where both of these designs are widely utilized. However, when giving forces simultaneously in vertical and horizontal directions, a choice must be regarding bird orientation. Algorithms must be developed to calculate optimal bird orientations for combinations of horizontal and vertical bird force requirements. Industry bird designs could be implemented in the simulation; however, this should ideally include the actual algorithms for bird orientation decision.

Acknowledgments

This work is part of an ongoing Industrial PhD at NMBU (Ås, Norway) for Geograf AS (Sandnes, Norway), by the corresponding author. It is funded by Geograf AS and the Research Council of Norway through their Industrial PhD program, project number 234875.

Corresponding author is presently on leave to Laboratório de Ondas e Correntes (LOC) at UFRJ/COPPE (Rio de Janeiro, Brazil).

Mr. Ken Welker of Geograf AS has contributed with helpful discussions and manuscript improvements.

References

Ablow, C. M. & Schechter, S. 1983. Numerical simulation of Undersea Cable Dynamics. *Ocean Engineering,* 10(6), 443–457.

Buia, M., Flores, P. E., Hill, D., Palmer, E., Ross, R., Walker, R., Houbiers, M., Thompson, M., Laura, S. & Menlikli, C. 2008. Shooting seismic surveys in circles. *Oilfield Review,* 20(3), 18–31.

Burgess, J. J. 1991. Modeling of Undersea Cable Installation with a Finite Difference Method. Proc. First International Offshore and Polar Engineering Conference, Edinburgh, UK, pp. 222–227.

Cebeci, T., Shao, J. P., Kafyeke, F. & Laurendeau, E. 2005. *Computational Fluid Dynamics for Engineers*. Long Beach, CA: Horizons Publishing. ISBN: 978-3-540-24451-6.

Ersdal, S. 2004. *An Experimental Study of Hydrodynamic Forces on Cylinders and Cables in Near Axial Flow*. PhD, Norwegian University of Science and Technology.

Gobat, J. I. & Grosenbaugh, M. A. 2006. Time-domain numerical simulation of ocean cable structures. *Ocean Engineering,* 33(10), 1373–1400.

Grant, T. J. 2015. The vertical shape of a buoyant acoustic streamer between depth control units. *Ocean Engineering,* 105, 176–185.

Grindheim, J. V., Revhaug, I. & Pedersen, E. 2017. Utilizing the EnKF (Ensemble Kalman Filter) and EnKS (Ensemble Kalman Smoother) for Combined State and Parameter Estimation of a 3D Towed Underwater Cable Model. *Journal of Offshore Mechanics and Arctic Engineering*, 139(6), 061303. DOI: 10.1115/1.4037173

James, G., David Burley, Dick Clements, Phil Dyke, John Searl, Steele, N. & Wright, J. 2011. *Advanced Modern Engineering Mathematics, 4th ed.* England, Pearson Education Limited, Prentice Hall.

Matlab, The language of technical computing. Natick, MA: The MathWorks, Inc.

Milinazzo, F., Wilkie, M. & Latchman, S. A. 1987. An efficient Algorithm for simulating the Dynamics of Towed Cable Systems. *Ocean Engineering,* 14(6), 513–526.

Newman, J. N. 1977. *Marine Hydrodynamics*. Cambridge, MA, The MIT Press. ISBN: 978-0-262-14026-3.

Orcina 2016. Orcaflex. Ulverston, Cumbria, UK: Orcina Ltd.

Pedersen, E. 2001. On the effect of slowly-varying course fluctuations of seismic vessels during towed multi-streamer operations. *Journal of Japan Institute of Navigation,* 104, 95–101.

Polydorides, N., Storteig, E. & Lionheart, W. 2008. Forward and inverse problems in towed cable hydrodynamics. *Ocean Engineering*, 35(14), 1429–1438.

Seatex, K. 2013a. *eBird – Seismic cable control* [Online]. Trondheim, Norway: Kongsberg Seatex. Available: https://www.km.kongsberg.com/ks/web/nokbg0240.nsf/AllWeb/EB747DB0D24FFF94C125765600465A3B?OpenDocument [Accessed 8 June 2017].

Seatex, K. 2013b. *Lateral steering and depth control of seismic streamers* [Online]. Trondheim, Norway: Kongsberg Seatex. Available: https://www.km.kongsberg.com/ks/web/nokbg0397.nsf/AllWeb/F34C5DEAD-3898F14C125764D004A3456/$file/eBird_oct09.pdf?OpenElement [Accessed 8 June 2017].

Solheim, P. 2013. *Method for determining correction under steering of a point on a towed object towards a goal position*. U.S. Patent 8,606,440, issued December 10, 2013.